Chemical Science

ROYAL SOCIETY OF CHEMISTRY

EDGE ARTICLE

View Article Online
View Journal | View Issue

Check for updates

Cite this: *Chem. Sci.*, 2026, **17**, 2772

All publication charges for this article have been paid for by the Royal Society of Chemistry

Received 3rd November 2025
Accepted 29th November 2025

DOI: 10.1039/d5sc08526h

rsc.li/chemical-science

Boraindenes as versatile precursors to benzannulated boron heterocycles

Nele Wieprecht,[ab] Ivo Krummenacher,[ab] Leonie Wüst,[ab] Maximilian Michel,[ab] Marco Neder,[ab] Andreas Häfner,[ab] Jordan Karg[ab] and Holger Braunschweig *[ab]

Five-membered boroles and their doubly benzannulated 9-borafluorene derivatives are established precursors for synthesizing various boron-doped heterocycles of broad applied interest. Extending this chemistry, we show that a series of 1-aryl-substituted boraindenes – the mono-benzannulated analogues of boroles – can similarly generate diverse boracycles *via* insertion of various substrates into their five-membered BC_4 ring. Insertion of chalcogens (O, S, Se), alkynes and an aryl azo compound yields boraindene-derived products that are distinguished from earlier examples by their unique ring-fusion patterns, thereby broadening the structural diversity within this class of boron heterocycles. Notably, these transformations provide access to unprecedented boron–sulfur and boron–selenium naphthalene analogues, while azobenzene insertion into the boraindene framework yields two distinct diazaborepin isomers.

Open Access Article. Published on 02 December 2025. Downloaded on 4/7/2026 6:27:18 PM.
This article is licensed under a Creative Commons Attribution-NonCommercial 3.0 Unported Licence.

Introduction

Boroles are a distinct class of five-membered boron heterocycles in which π-conjugation between a three-coordinate boron center and a butadienediyl carbon framework generates an antiaromatic system.[1] This unique electronic structure, characterized by a narrow HOMO–LUMO gap, coupled with strong Lewis acidity and electron-accepting capabilities, renders boroles attractive building blocks in materials chemistry.[2] These advantageous properties can be further tuned through functionalization of ring substituents or incorporation into extended π systems, strategies that simultaneously mitigate the inherent instability and high reactivity of the borole core.[1,2]

Beyond their fascinating electronic and optical features, boroles serve as versatile synthetic precursors for diverse aromatic and non-aromatic boron ring structures.[3] For instance, they readily undergo ring expansion reactions with unsaturated substrates, efficiently generating larger boron-containing heterocycles such as six-membered 1,2-azaborinines (boron-nitrogen analogues of benzene)[4] and seven-membered borepins[5] – structural motifs with promise for optoelectronic applications.[2,4,5] While boroles (**A**) and their bis-benzannulated derivatives, 9-borafluorenes (**C**), have been thoroughly explored for such transformations, the mono-benzannulated 1-boraindene analogues (**B**) remain largely overlooked (Fig. 1).

The first reported derivative, a 1-chloro-substituted boraindene synthesized by Kaufmann *via* pyrolysis in 1987, was too reactive for isolation but exhibited characteristic borole insertion reactivity in both alkyne trapping reactions and self-dimerization.[6] Decades later, the Piers group exploited the unique reactivity of a perfluorinated boraindene in the activation of both H–H and H–Si bonds, thereby demonstrating its versatility in σ-bond activation chemistry.[7–9] To further develop the chemistry of the boraindene system, we recently reported the synthesis of 1,2,3-triphenyl-1-boraindene (**1Ph**, Fig. 2) and demonstrated how its distinct molecular framework imparts unique Lewis acidic, optical, electronic and antiaromatic characteristics.[10] Initial reactivity studies with organic azides revealed facile nitrogen atom insertion to form 2,1-azaboranaphthalenes, the benzannulated analogues of 1,2-azaborinines.[10]

Inspired by these findings and the broader synthetic potential of 1-boraindenes as precursors to benzannulated boron heterocycles, we now report three new derivatives bearing chloro, *p*-tolyl, and duryl substituents on the boron atom, and expand our reactivity studies to encompass chalcogens, alkynes,

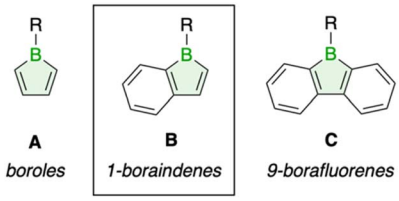

Fig. 1 Representative examples of borole frameworks with increasing degrees of benzannulation, from monocyclic boroles (**A**) over bicyclic 1-boraindenes (**B**) to tricyclic 9-borafluorene systems (**C**).

[a]*Institute for Inorganic Chemistry, Julius-Maximilians-Universität Würzburg, Am Hubland, 97074 Würzburg, Germany. E-mail: h.braunschweig@uni-wuerzburg.de*
[b]*Institute for Sustainable Chemistry & Catalysis with Boron, Julius-Maximilians-Universität Würzburg, Am Hubland, 97074 Würzburg, Germany*

© 2026 The Author(s). Published by the Royal Society of Chemistry

Open Access Article. Published on 02 December 2025. Downloaded on 4/7/2026 6:27:18 PM.
This article is licensed under a Creative Commons Attribution-NonCommercial 3.0 Unported Licence.

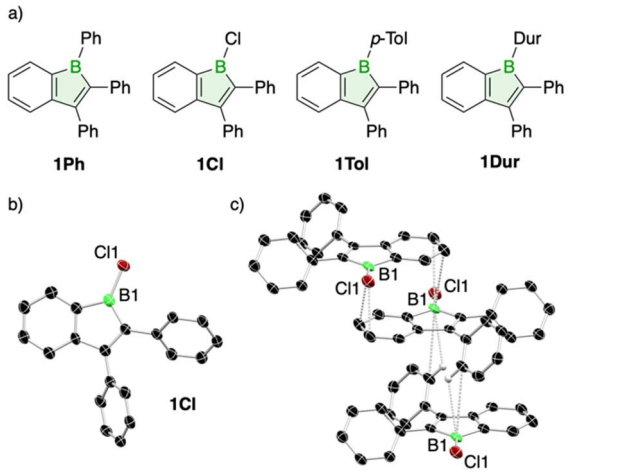

Fig. 2 (a) The previously reported 1,2,3-triphenyl-1-boraindene **1Ph** and new derivatives bearing 1-chloro (**1Cl**), 1-*p*-tolyl (**1Tol**), and 1-duryl (**1Dur**) substituents at the boron center. (b) Molecular structure of **1Cl** with thermal ellipsoids at 50% probability and (c) depiction of close intermolecular contacts within the crystal packing of **1Cl**. Hydrogen atoms are omitted for clarity, except those involved in intermolecular interactions. The molecular structure of **1Dur** is provided in the SI.

and azobenzene. These investigations furnished the first boron–sulfur and boron–selenium naphthalene analogues, along with benzannulated borepin derivatives from alkyne reactions, revealing a pronounced preference of these 1-boraindenes for endocyclic B–C insertion over cycloaddition with alkynes. Reactions with azobenzene unveiled a sterically-governed pathway, affording distinct diazaborepin isomers depending on the boron substituent. These findings establish fundamental reactivity patterns of 1-boraindenes and highlight their versatility as platforms for the synthesis of diverse boron heterocycles, offering new routes to both known and previously inaccessible derivatives.

Results and discussion

Preparation of new 1-boraindene derivatives

Our work extends 1-boraindene chemistry through the synthesis of three new derivatives (Fig. 2). In a similar manner to the previously reported 1,2,3-triphenyl-1-boraindene (**1Ph**),[10] both the 1-*p*-tolyl (**1Tol**) and 1-chloro derivatives (**1Cl**) were prepared efficiently *via* tin-boron exchange between 1,1-dimethyl-2,3-diphenyl-1-stannaindene[8] and the corresponding dibromoborane $RBBr_2$ (R = *p*-tolyl)[11] or BCl_3, with yields above 76%. The 1-duryl derivative **1Dur**, not accessible *via* this route, was obtained from **1Cl** by reaction with duryl lithium in 79% yield. The distinct nature of the duryl derivative is reflected in its ^{11}B NMR signal at 74.8 ppm, which is significantly downfield-shifted compared to those of the other derivatives, clustered in a narrow range between 65.0 and 65.5 ppm. This marked difference is most likely attributable to the steric demand of the duryl group, which disrupts π conjugation between boron and the exocyclic substituent. X-ray crystallographic analysis supports this conclusion, revealing that the duryl group adopts an orientation close to perpendicular (69.9°) relative to the boraindene ring, whereas the phenyl group in **1Ph** is considerably less twisted (32.6°). The *p*-tolyl derivative **1Tol** could not be included in the comparison, as all attempts to obtain single crystals were unsuccessful. The B–Cl bond length in **1Cl** (1.747(5) Å) falls within the expected range, as do the remaining structural parameters of this haloborole derivative (Fig. 2).[12–14] Crystal packing analysis reveals weak intermolecular interactions between the boron atom and the π system of neighboring benzene rings, with the shortest B···C contact at 3.453(7) Å. Additionally, the Lewis-acidic boron atom engages in an interaction with the C–H bond of a neighboring exocyclic phenyl group (CH···B 2.928 Å), leading to a stacked molecular arrangement (Fig. 2). Notably, comparable intermolecular boron contacts are also present in the crystal structure of 9-chloro-9-borafluorene.[12]

In contrast to the less sterically protected 1-chloro-1-boraindene reported by Kaufmann,[6] which bears only hydrogen substituents, and the monocyclic 1-chloro-2,3,4,5-tetraphenylborole,[13,15] **1Cl** is remarkably stable both in solution and the solid state, showing no signs of decomposition or dimerization at room temperature and elevated temperatures. A related benzannulated derivative of **1Cl**, 9-chloro-9-borafluorene, also exhibits striking stability, as evidenced by its ability to be purified by distillation at 90 °C.[12]

To evaluate the effect of the different boron substituents on Lewis acidity, we employed the Gutmann–Beckett NMR method in benzene solution.[16] Adducts with one equivalent of triethylphosphine oxide ($OPEt_3$) formed readily for **1Cl** and **1Tol**, resulting in ^{31}P NMR signals at 77.6 and 75.4 ppm, respectively. In contrast, the duryl derivative **1Dur** forms only a weak adduct at room temperature, with an averaged ^{31}P NMR resonance at 49.9 ppm, likely due to steric shielding of the Lewis-acidic boron center by the *ortho* methyl groups. This value increases with decreasing temperature, and at −80 °C in toluene-d_8 solution the ^{31}P NMR signal shifts to 73.2 ppm, indicating complete adduct formation. Analysis of the resulting acceptor numbers (AN) demonstrates that chloroboraindene **1Cl** is the strongest Lewis acid (AN = 80.8) in the series, followed by **1Ph** (AN = 76.9) and **1Tol** (AN = 76.1), which display progressively lower Lewis acidity. The AN value for **1Dur** (AN = 71.1) cannot be directly compared to the others, as it was obtained under different conditions (−80 °C in toluene *vs.* room temperature in benzene). Nonetheless, it aligns with the expected trend of decreasing Lewis acidity corresponding to the weaker π-accepting ability of more electron-rich aryl substituents.

Building on the well-established tendency of boroles to undergo functionalization reactions that relieve the destabilizing 4π-electron system and drive the formation of larger heterocycles, we investigated the reactivity of the 1-aryl derivatives toward chalcogens, alkynes, and azobenzene. These transformations effected ring expansion and produced new benzannulated boron heterocycles.

Chalcogen insertions

By inserting chalcogens into boraindenes, we aimed to access aromatic boron-chalcogen naphthalene analogues, fundamental structural motifs that had previously been reported only for the lightest chalcogen, oxygen.[17,18]

Open Access Article. Published on 02 December 2025. Downloaded on 4/7/2026 6:27:18 PM.
This article is licensed under a Creative Commons Attribution-NonCommercial 3.0 Unported Licence.

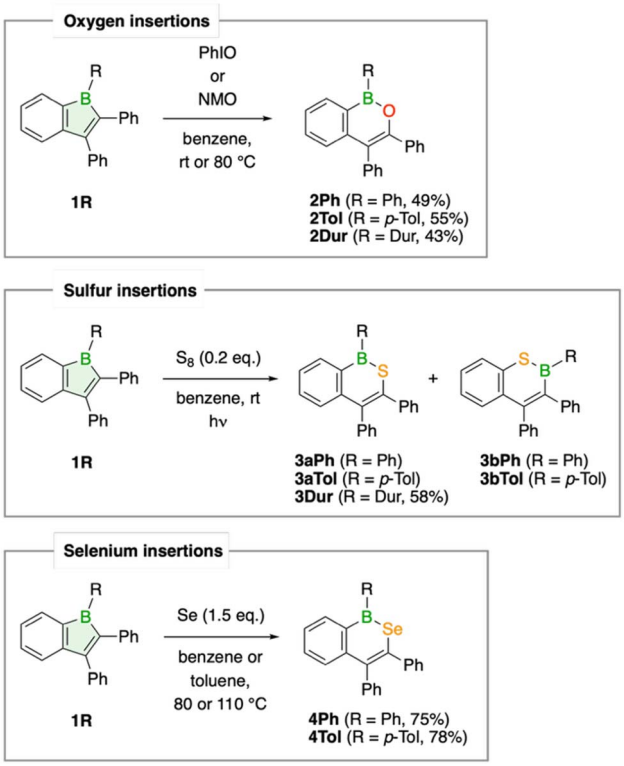

Scheme 1 Synthesis of B,E-naphthalenes *via* chalcogen atom (*E* = O, S, Se) insertion into 1-aryl-1-boraindenes **1R** (R = Ph, *p*-Tol, Dur).

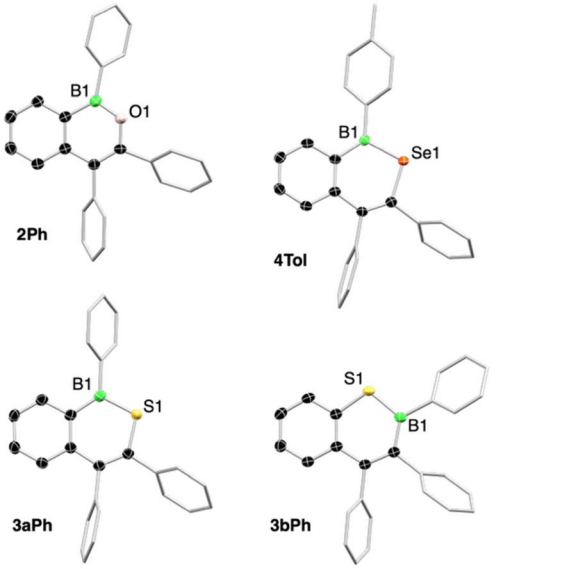

Fig. 3 Selected molecular structures showing the chalcogen insertion products **2Ph**, **3aPh**, **3bPh**, and **4Tol** with thermal ellipsoids drawn at the 50% probability level. Thermal ellipsoids for the aryl substituents and all hydrogen atoms have been omitted for clarity. Depictions of the molecular structures for **2Tol**, **2Dur**, **3Tol**, and **3Dur** are provided in the SI.

Treatment of the 1-boraindenes **1Ph**, **1Tol**, and **1Dur** with either iodosobenzene or *N*-methylmorpholine *N*-oxide afforded the corresponding oxygen-atom-expanded ring systems as white solids in yields ranging from 43 to 55% (Scheme 1). The transformation to 1,2-B,O-naphthalenes is readily observed by decolorization of the red boraindene solution and confirmed by the more shielded ^{11}B NMR resonances, resulting from the π-donating effect of the oxygen atom. Compounds **2Ph**, **2Tol**, and **2Dur** exhibit ^{11}B NMR chemical shifts tightly grouped between 42.0 and 44.2 ppm, consistent with related structures by Martin, Wagner and Dong.[18–22] The structures of all three compounds have been determined by X-ray diffraction analysis, confirming their naphthalene-like framework. The B–O bond lengths (1.377(2)–1.383(3) Å) are consistent with those reported for a related B,O-containing naphthalene derivative prepared by an alternative synthetic route.[18] As observed in the boraindene **1Dur**, the duryl substituent in **2Dur** is twisted nearly perpendicular (80.5°) to the plane of the bicyclic core due to steric hindrance, whereas the other aryl boron substituents show a lesser degree of twisting, namely 45.9° for **2Tol** and 46.7° for **2Ph** (Fig. 3).

The sulfur analogues, **3R**, were obtained by irradiating **1R** (R = Ph, *p*-Tol, Dur) in benzene with elemental sulfur for 16 h to 3 days, depending on the aryl substituent (Scheme 1). The ^{11}B NMR resonances of the pale-yellow derivatives **3Ph**, **3Tol**, and **3Dur** appear between 56.6 and 59.4 ppm and fall within the expected range for such compounds.[23–25] A closer analysis by NMR spectroscopy revealed that the insertion reaction for the phenyl and *p*-tolyl derivatives proceeds non-selectively, producing regioisomeric products **3bR** alongside the expected insertion products **3aR** (R = Ph, *p*-Tol). The 1,2-B,S isomers **3aR**, in which the sulfur atom inserts into the endocyclic B–C bond opposite the benzo substituent, predominate in both cases. In contrast, the sterically more demanding duryl derivative **1Dur** converts cleanly to the expected sulfur insertion product, the 1,2-B,S isomer **3Dur**, which was isolated as a pale-yellow solid in 58% yield. While only an isomeric mixture of isomers **3aTol** and **3bTol** could be isolated for the *p*-tolyl derivative, the major 1,2-B,S isomer **3aPh** for the phenyl derivative could be separated in analytically pure form in 15% yield. Assignment and characterization of the different regioisomers were achieved by X-ray crystallographic analysis (Fig. 3).

The isomers can also be readily distinguished by characteristic through-space interactions between the boron-bound aryl group and neighboring protons, as observed in the 2D ^{1}H–^{1}H NOESY experiment (see SI for details). Both isomers of the phenyl derivative could be structurally characterized, whereas only isomer **3bTol** of the *p*-tolyl derivative was accessible by single-crystal X-ray diffraction. The B–S bond lengths in the structures are essentially identical, ranging from 1.788(4) to 1.791(2) Å, and reflect significant π-delocalization comparable to that found in BSC_4 rings exhibiting aromatic character.[23,24]

Incorporation of the heavier chalcogen selenium into **1R** to generate boron-selenium-containing naphthalene analogues were achieved by reaction of **1Ph** and **1Tol** with elemental selenium (Scheme 1). When a benzene solution of **1Ph** was heated with a slight excess of red selenium (1.5 equiv) at 80 °C for three days, the solution gradually changed color from red to orange, and a new ^{11}B NMR resonance appeared at 63.6 ppm, consistent with formation of the insertion product **4Ph**.

© 2026 The Author(s). Published by the Royal Society of Chemistry

Open Access Article. Published on 02 December 2025. Downloaded on 4/7/2026 6:27:18 PM. This article is licensed under a Creative Commons Attribution-NonCommercial 3.0 Unported Licence.

Formation of the *p*-tolyl derivative **4Tol** did not proceed under the same conditions, requiring heating at 110 °C in toluene, whereas no formation of the duryl derivative **4Dur** was observed even at 120 °C. Unlike the sulfur insertion reactions, these selenium insertions are selective, producing exclusively a single product. Compound **4Tol** exhibits a ^{11}B NMR signal at 64.0 ppm. Good isolated yields of 75% (**4Ph**) and 78% (**4Tol**) were achieved for both insertion products. The ^{77}Se NMR signals were observed at 479 (**4Ph**) and 475 ppm (**4Tol**), respectively, in good agreement with the value reported for a boron–selenium-containing phenanthrene analogue ($\delta(^{77}\mathrm{Se})$ = 494 ppm).[23] Compound **4Tol** was further characterized by single-crystal X-ray diffraction. Suitable crystals were obtained by layering a saturated toluene solution of **4Tol** with pentane at −30 °C. Structural parameters of the planar $BSeC_4$ unit closely resemble those of the B,Se-phenanthrene derivative, with a B–Se bond length of 1.915(4) Å and a small C–Se–B bond angle of 101.4(1) ° at the selenium atom (Fig. 3).[23]

The observed trend of decreased shielding of the ^{11}B NMR resonances down the chalcogen group, exemplified by resonances at 43.5, 57.3, and 63.6 ppm for **2Ph**, **3Ph** and **4Ph**, respectively, can be explained by the progressively weaker π-donation from the lone pairs of the heavier chalcogen atoms to the empty boron p orbital. Related studies of 9-borafluorene derivatives have shown a similar ^{11}B NMR chemical shift progression across the chalcogen series.[23] The aromaticity of the boracycles, evaluated by nucleus-independent chemical shifts (NICS),[26] indicates comparable aromatic character among the derivatives: **2Ph** ($NICS_{zz}(-1/1) = -7.05$), **3Ph** ($NICS_{zz}(-1/1) = -9.30$), and **4Ph** ($NICS_{zz}(-1/1) = -7.87$). While shielding effects from the heavier chalcogens are expected to influence NICS values, a comparison of the sulfur derivative **3Ph** with its non-annulated pentaphenyl-1,2-thiaborinine analogue ($NICS(1)_{zz} = -12.75$ ppm)[24] and benzannulated 10-phenyl-10,9-borathiaphenanthrene analogue ($NICS(-1/1)_{zz} = -2.84$ ppm)[23] reveals that aromaticity in the boracycle decreases with increasing benzannulation, consistent with expected trends. Moreover, the differences in aromaticity between the 1,2- and 2,1-B,E isomers (*E* = O, S, Se) are minimal, which is consistent with their only slight differences in thermodynamic stability. For example, the 1,2-B,S isomer, observed in the sulfur insertion reaction of **1Ph**, was found to be more stable than its 1,2-counterpart by merely +0.47 kcal mol^{-1} (see SI for details). To gain richer spatial insight into the conjugation and aromaticity of the derivatives, we analyzed the anisotropy of the current (induced) density (ACID, Fig. 4).[27] Visualizations of the current density reveal diatropic (aromatic) ring currents that become progressively disrupted with heavier chalcogen substitution, indicating a gradual loss of aromaticity in contrast to the trends suggested by the NICS values (Fig. 4). The selenium derivative exhibits discontinuous induced current loops that are interrupted at the chalcogen position, reflecting a loss of aromatic stabilization.

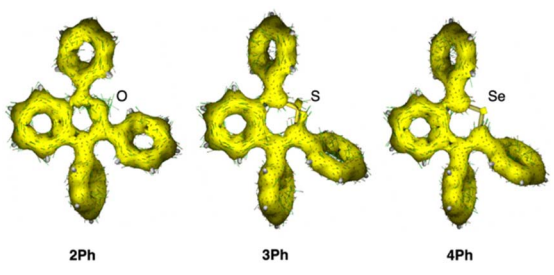

Fig. 4 ACID isosurfaces of compounds **2Ph**, **3Ph**, and **4Ph** displaying σ and π contributions at an isovalue 0.050 a.u. The magnetic field is applied perpendicular to the molecular plane of the annulated ring system. Current density vectors are overlaid on the ACID isosurfaces to illustrate diatropic (aromatic) ring currents.

Alkyne insertions

We further explored the reaction of boraindenes **1Ph** and **1Tol** with alkynes, a classic and characteristic reactivity pattern of boroles, documented for non-, mono-, and bis-benzannulated derivatives.[6,28–39] The reaction can proceed through multiple pathways, producing diverse products such as seven-membered borepins and bicyclic boranorbornadienes.

Both the phenyl- and *p*-tolyl-substituted boraindenes were found to react with diphenylacetylene at room temperature to give the borepins **5Ph^{Ph}** and **5Tol^{Ph}** in good isolated yields of 83% and 82%, respectively (Scheme 2). Monitoring the reaction indicated completion over 4 days, with no observable

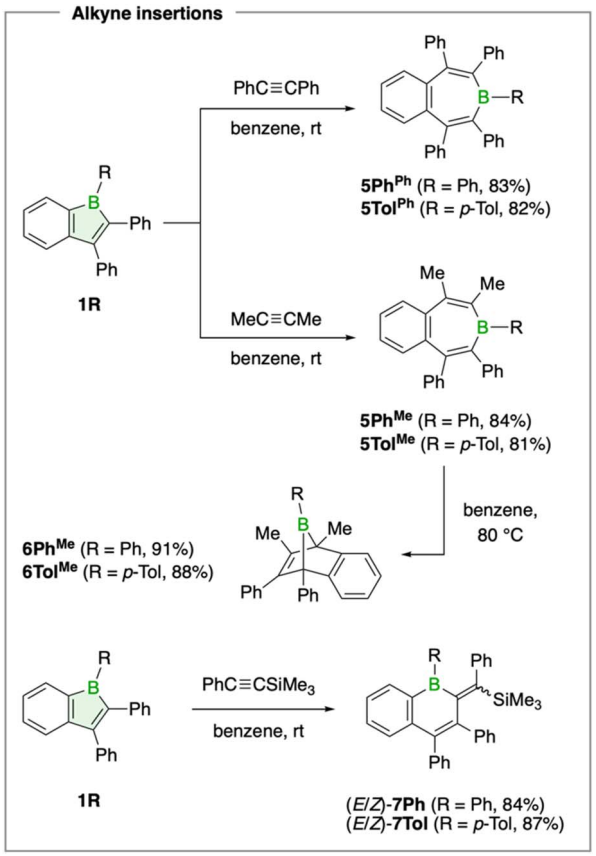

Scheme 2 Products obtained from the reaction of aryl-substituted 1-boraindenes **1Ph** and **1Tol** with symmetrical and unsymmetrical alkynes.

Open Access Article. Published on 02 December 2025. Downloaded on 4/7/2026 6:27:18 PM.
This article is licensed under a Creative Commons Attribution-NonCommercial 3.0 Unported Licence.

intermediates. The products, obtained as white solids, exhibit ^{11}B NMR signals at 72.1 ppm (**5Ph^{Ph}**) and 71.5 ppm (**5Tol^{Ph}**), consistent with the expected range for tricoordinate boron atoms in borepins.[33,36,37,40] Similar reactivity was observed with 2-butyne (dimethylacetylene), which afforded the corresponding borepins **5Ph^{Me}** (84% yield, $\delta(^{11}B) = 68.3$ ppm) and **5Tol^{Me}** (81%, $\delta(^{11}B) = 69.2$ ppm).

The seven-membered rings in all four borepin structures, as determined by X-ray diffraction analysis, adopt nonplanar boat conformations that disrupt delocalization within the ring, consistent with previous observations for aryl-substituted borepins.[30,33,37] The carbon–carbon bond lengths within the ring further indicate minimal π conjugation, showing values characteristic of localized single and double bonds.

Next, we investigated the thermal stability of the borepins to determine whether alternative isomeric forms are accessible. The aryl-substituted borepins **5Ph^{Ph}** and **5Tol^{Ph}** remained unchanged, whereas the methyl derivatives **5Ph^{Me}** and **5Tol^{Me}** gradually converted at 80 °C over 4 days into new species exhibiting ^{11}B NMR resonances at −5.2 and −4.4 ppm (Scheme 2). The pronounced upfield shifts are consistent with the formation of bicyclic 7-boranorbornadiene structures, stabilized by intramolecular interaction between the electron-deficient boron atom and the non-conjugated C=C double bond.[29–32,38] Single-crystal X-ray diffraction analysis of crystals obtained by slow evaporation of saturated pentane solutions at −30 °C confirmed the proposed structures, which correspond to the formal [4 + 2] Diels–Alder cycloaddition product of the corresponding boraindenes with 2-butyne. Compound **6Ph^{Me}** crystallizes with two molecules in the unit cell, each exhibiting different geometric parameters, which can be attributed to two distinct orientations of the phenyl substituent on the bridgehead boron atom (Fig. 5). While both BPh units are markedly tilted toward the non-annulated double bond, in one conformation the phenyl group is oriented roughly orthogonally to the axis defined by the carbon atoms of the C=C double bond, facilitating optimal overlap of the vacant boron p orbital and the π system. Despite the enhanced overlap, the C=C bond length in this conformation (1.388(3) Å) is not statistically different from that in the alternate conformation (1.373(3) Å), where the phenyl group is twisted relative to the double bond. The bridgehead boron bond angles are nearly identical in both conformations (97.6(2)° and 97.4(2)°), with values typical for these strained systems.[30–32,38] The crystal structure of **6Tol^{Me}** reveals a single conformation in the unit cell, with the *p*-tolyl group oriented approximately perpendicular to the axis defined by the double bond and markedly tilted toward it. The overall structural parameters closely match those of **6Ph^{Me}** in the same conformation.

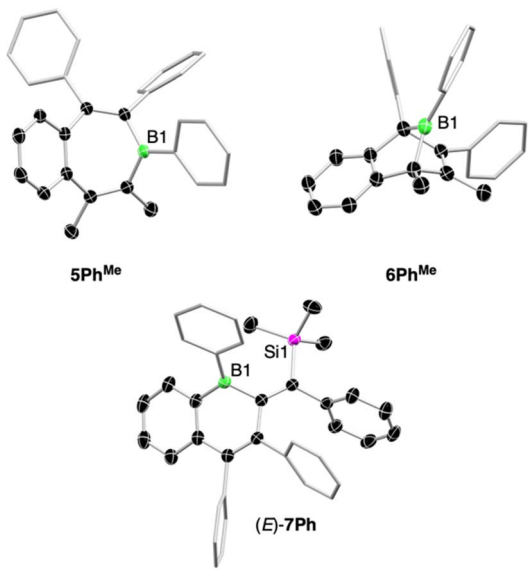

Fig. 5 Representative structures of the three distinct alkyne insertion products: 5Ph^{Me}, 6Ph^{Me}, and (*E*)-7Ph. Thermal ellipsoids are depicted at the 50% probability level; those for the aryl substituents are omitted. Hydrogen atoms have been excluded for clarity. Molecular structures for 5Ph^{Ph}, 5Tol^{Ph}, 5Tol^{Me}, 6Tol^{Me}, (*Z*)-7Ph and (*E*)-7Tol are provided in the SI.

The reactions of boraindenes with the methyl-substituted alkynes establish a clear order of thermodynamic stability among the isomeric products: at room temperature, the reaction proceeds *via* insertion to form seven-membered borepins, while upon heating, thermal isomerization occurs, yielding the bicyclic boranorbornadienes **6Ph^{Me}** and **6Tol^{Me}** as the thermodynamically favored species. This two-step pathway, consisting of insertion followed by rearrangement, offers an alternative to the direct [4 + 2] cycloaddition of the borole with the alkyne that forms the boranorbornadiene. We have proposed a similar competitive insertion mechanism for pentaphenylborole,[36] where boranorbornadiene formation was long assumed to proceed *via* a Diels–Alder pathway.[28] Although an insertion pathway is clearly favored for the boraindene–alkyne combinations reported here and in Kaufmann's previous study,[6] cycloaddition reactivity of boroles with alkynes has been unequivocally demonstrated elsewhere.[30] These findings highlight that both steric and electronic effects of the substituents on the alkyne and the borole govern the reaction pathway and ultimately determine the relative stability of the products, which can also interconvert.

The pronounced dependence on the nature of the substituents is further illustrated by the reaction of boraindenes **1Ph** and **1Tol** with the unsymmetrical alkyne 1-phenyl-2-trimethylsilylacetylene. Treatment of these boraindenes with one equivalent of the alkyne afforded an additional, distinct insertion product (Scheme 2). This transformation was accompanied by a gradual color change of the solution from red to orange over 3 days, along with new ^{11}B NMR signals at 71.4 ppm (**7Ph**) and 69.9 ppm (**7Tol**), respectively. The resulting yellow solids were isolated in yields of 84% (**7Ph**) and 87% yield (**7Tol**), respectively. Single-crystal X-ray diffraction revealed the ring expansion of the borole unit to form a boracyclohexadiene, a structural motif previously established in borole insertion chemistry (Fig. 5).[30,34] For **7Ph**, both the *E* and *Z* isomers, arising from different configurations of substituents across the exocyclic double bond on the six-membered boracycle, were observed. These correspond to isomers in which the silyl and boryl groups are either *cis* or *trans* to each other, respectively.

© 2026 The Author(s). Published by the Royal Society of Chemistry

Open Access Article. Published on 02 December 2025. Downloaded on 4/7/2026 6:27:18 PM. This article is licensed under a Creative Commons Attribution-NonCommercial 3.0 Unported Licence.

7Tol crystallized exclusively in the *E* conformation (Fig. 5). Overall, the structural parameters confirm the assignment of **7R** (R = Ph, *p*-Tol) as boron-containing dihydronaphthalene analogues. The two geometric isomers of **7Ph** and **7Tol** are readily distinguished by NMR spectroscopy. The observed isomeric ratio is approximately 2 : 1 for **7Ph** and 5 : 2 for **7Tol**, both favoring the *E* isomer in solution. The divergent insertion pathway, involving a one-carbon ring expansion of the borole unit to a boracyclohexadiene, is likely facilitated by a facile silyl migration that occurs after the initial adduct formation between the alkyne and the boron atom.[41]

Azobenzene insertion

Drawing on established reactivity patterns known from monocyclic boroles, we examined the reaction of boraindenes **1Ph**, **1Tol**, and **1Dur** with azobenzene.[42] In prior studies, photolytic reaction of pentaphenylborole with this aryl azo compound was shown to produce seven-membered 1,3,2-diazaborepin products,[42] BN analogues of azepines.[43]

When the boraindenes **1Ph** and **1Tol** were irradiated with UV light from a mercury lamp in the presence of one equivalent of azobenzene for 16 h at room temperature, selective formation of new products was observed, exhibiting ^{11}B NMR resonances at 32.7 ppm (**8Ph**) and 32.1 ppm (**8Tol**), respectively (Scheme 3). ^{11}B NMR spectroscopic monitoring indicated that the reaction proceeds without observable intermediates. The boron chemical shifts of these products align closely with that reported for a related fully phenyl-substituted 1,3,2-diazaborepin derivative ($\delta(^{11}B)$ = 31.6 ppm).[42] The formation of the benzannulated BN_2C_4 ring as the reaction product was confirmed by single-crystal X-ray diffraction analysis. Due to structural disorder in **8Ph**, bond parameters are discussed only for the *p*-tolyl derivative **8Tol** (Fig. 6). Analysis of **8Tol** reveals a nonplanar, boat-like conformation of the boracycle featuring two distinct B–N bonds characteristic of a σ bond (1.473(3) Å) and a dative π bond (1.409(3) Å).[44] The nitrogen atom not involved in π bonding exhibits slight pyramidalization, with an angular sum of 353.3(3)°. Overall, the structural parameters of **8Tol** are closely

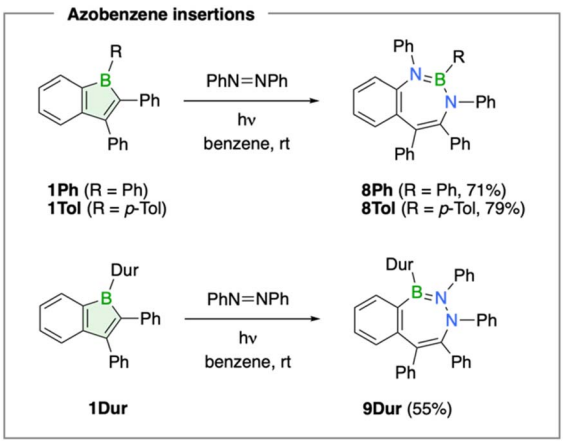

Scheme 3 Synthesis of diazaborepins *via* azobenzene insertion into boraindenes **1Ph**, **1Tol**, and **1Dur**.

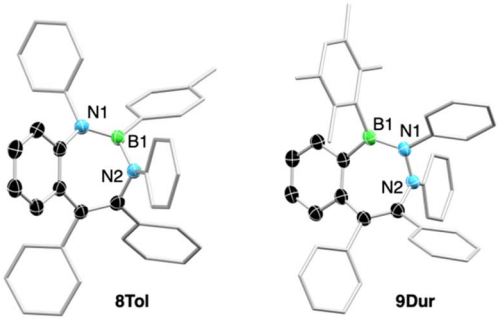

Fig. 6 Molecular structures of **8Tol** and **9Dur** with thermal ellipsoids at the 50% probability level; those for the aryl substituents are omitted. Hydrogen atoms have been excluded for clarity. The molecular structure of **8Ph** is shown in the SI.

comparable to those reported for the perphenylated derivative by the Martin group.[42]

Interestingly, the reaction of the duryl derivative **1Dur** with azobenzene under similar conditions led to a different outcome, as indicated by the significantly downfield-shifted ^{11}B NMR signal at 46.3 ppm for the isolated product **9Dur** (55% yield, Scheme 3). X-ray diffraction analysis revealed a seven-membered BN_2C_4 boracycle with an intact N–N bond, formed by the formal insertion of azobenzene into the endocyclic B–C bond opposite the benzo group (Fig. 6). The boracycle adopts a more twisted boat conformation compared to those observed for **8Ph** and **8Tol**. The two phenyl groups across the N–N single bond (1.421(3) and 1.433(2) Å) are mutually *trans*, with C–N–N–C endocyclic torsion angles of 98.3(2) and 106.7(2)° for the two independent molecules in the unit cell. The B–N bond lengths of 1.419(2) and 1.420(2) Å are characteristic of significant double bond character.[44]

Although seven-membered 1,3,2-diazaborepin products such as **8Ph** and **8Tol** have been previously reported from the reaction of pentaphenylborole with azo compounds,[42] the direct insertion of an azo group into the borole unit of **1Dur** to form **9Dur** represents an unprecedented transformation – one analogous to alkyne insertion that results in formal 1,2-carboboration of the unsaturated N=N bond. Thus, depending on the steric demand of the aryl boron substituent, the photochemical reaction of boraindenes with azobenzene affords two distinct isomeric forms of B,N-azepine. Notably, **9Dur**, featuring a B–N–N connectivity within the ring, represents an unprecedented structural motif among diazaborepins.

Conclusions

In summary, we have expanded the range of known boraindene derivatives by synthesizing 1-*p*-tolyl, 1-duryl, and 1-chloro variants, all sharing the characteristic 2,3-diphenyl-substituted backbone. Insertion of chalcogen atoms into the boraindenes afforded B,O-, B,S-, and B,Se-naphthalenes, thereby adding previously unknown sulfur and selenium derivatives to this family. The reactivity of the boraindenes with various alkynes under thermal conditions demonstrated a preference for an insertion pathway, initially yielding stable borepin derivatives.

Open Access Article. Published on 02 December 2025. Downloaded on 4/7/2026 6:27:18 PM. This article is licensed under a Creative Commons Attribution-NonCommercial 3.0 Unported Licence.

At elevated temperatures, the dimethyl-substituted borepins derived from 2-butyne rearrange into bicyclic boranorbornadienes, which are the formal [4 + 2] cycloaddition products of boraindenes and alkynes and represent the thermodynamically favored species. Reaction with 1-phenyl-2-trimethylsilylacetylene induced one-carbon insertion and ring expansion to form a boracyclohexadiene ring featuring an exocyclic double bond, a structural motif previously reported in monocyclic borole derivatives. Lastly, the aryl-substituted boraindenes reacted with diazobenzene to form diazaborepins (or BN-azepines), with the isomer outcome influenced by the steric bulk of the 1-aryl substituent. Notably, the 1-duryl derivative undergoes a formal 1,2-carboboration through insertion of the azo group, resembling the mechanism observed in borepin formation from alkynes. These reactions establish boraindenes as versatile precursors to heteroatom-doped polycyclic compounds, offering synthetic access to scaffolds that complement those derived from boroles and 9-borafluorenes. Future studies will further exploit their potential and elucidate differences between monocyclic boroles and tricyclic 9-borafluorene analogues.

Author contributions

N. W.: conceptualization, methodology, investigation. I. K.: writing-original draft preparation, visualization. L. W.: formal analysis. M. M: formal analysis. M. N.: formal analysis. A. H.: formal analysis. J. K.: investigation. H. B.: supervision.

Conflicts of interest

There are no conflicts to declare.

Data availability

CCDC 2499789–2499810 (**1Cl**, **1Dur**, **2Dur**, **2Ph**, **2Tol**, **3Dur**, **3aPh**, **3bPh**, **3bTol**, **4Tol**, **5Ph^{Me}**, **5Ph^{Ph}**, **5Tol^{Me}**, **5Tol^{Ph}**, **6Ph^{Me}**, **6Tol^{Me}**, *E*-**7Ph**, *Z*-**7Ph**, *E*-**7Tol**, **8Ph**, **8Tol**, and **9Dur**). contain the supplementary crystallographic data for this paper.[45a–v]

The data supporting the findings of this study are available in the supplementary information (SI) of this article. Supplementary information is available. See DOI: https://doi.org/10.1039/d5sc08526h.

Acknowledgements

We thank the Julius-Maximilians-Universität Würzburg and the Deutsche Forschungsgemeinschaft (DFG grant 466754611) for financial support of this work.

Notes and references

1 For general borole reviews, see:(*a*) J. J. Eisch, *Adv. Organomet. Chem.*, 1996, **39**, 355–391; (*b*) A. Steffen, R. M. Ward, W. D. Jones and T. B. Marder, *Coord. Chem. Rev.*, 2010, **254**, 1950–1976; (*c*) H. Braunschweig and T. Kupfer, *Chem. Commun.*, 2011, **47**, 10903–10914; (*d*) H. Braunschweig, I. Krummenacher and J. Wahler, *Adv. Organomet. Chem.*, 2013, **61**, 1–53; (*e*) B. Su and R. Kinjo, *Synthesis*, 2017, **49**, 2985–3034; (*f*) C. Hong, J. Baltazar and J. D. Tovar, *Eur. J. Org Chem.*, 2022, e202101343.

2 (*a*) F. Jäkle, *Chem. Rev.*, 2010, **110**, 3985–4022; (*b*) S. Kervyn, C. Aurisicchio and D. Bonifazi, in *Functional Supramolecular Architectures*, ed. P. Samorì and F. Cacialli, Wiley-VCH, Weinheim, 2011, ch. 8, pp. 233–280; (*c*) A. Escande and M. J. Ingleson, *Chem. Commun.*, 2015, **51**, 6257–6274; (*d*) Y. Ren and F. Jäkle, *Dalton Trans.*, 2016, **45**, 13996–14007; (*e*) L. Ji, S. Griesbeck and T. B. Marder, *Chem. Sci.*, 2017, **8**, 846–863; (*f*) W. Zhang, B. Zhang, D. Yu and G. He, *Sci. Bull.*, 2017, **62**, 899–900; (*g*) A. Wakamiya, in *Main Group Strategies Towards Functional Hybrid Materials*, ed. T. Baumgartner and F. Jäkle, John Wiley & Sons Ltd, Hoboken (New Jersey), 2018, vol. 1, pp. 1–26; (*h*) E. v. Grotthuss, A. John, T. Kaese and M. Wagner, *Asian J. Org. Chem.*, 2018, **7**, 37–53; (*i*) J. He, F. Rauch, M. Finze and T. B. Marder, *Chem. Sci.*, 2021, **12**, 128–147.

3 (*a*) J. H. Barnard, S. Yruegas, K. Huang and C. D. Martin, *Chem. Commun.*, 2016, **52**, 9985–9991; (*b*) Y. Su and R. Kinjo, *Chem. Soc. Rev.*, 2019, **48**, 3613–3659; (*c*) X. Su, T. A. Bartholome, J. R. Tidwell, A. Pujol, S. Yruegas, J. J. Martinez and C. D. Martin, *Chem. Rev.*, 2021, **121**, 4147–4192; (*d*) X. Li, Y.-M. Chen and Z.-G. Xu, *Org. Chem. Front.*, 2025, **12**, 3521–3533.

4 (*a*) M. J. D. Bosdet and W. E. Piers, *Can. J. Chem.*, 2009, **87**, 8–29; (*b*) P. G. Campbell, A. J. V. Marwitz and S.-Y. Liu, *Angew. Chem., Int. Ed.*, 2012, **51**, 6074–6092; (*c*) G. Bélanger-Chabot, H. Braunschweig and D. K. Roy, *Eur. J. Inorg. Chem.*, 2017, 4353–4368; (*d*) Z. X. Giustra and S.-Y. Liu, *J. Am. Chem. Soc.*, 2018, **140**, 1184–1194.

5 (*a*) R. E. Messersmith and J. D. Tovar, *J. Phys. Org. Chem.*, 2015, **28**, 378–387; (*b*) L. Wang, J. Ma, E. Si and Z. Duan, *Synthesis*, 2021, **53**, 623–635.

6 W. Schacht and D. Kaufmann, *Angew. Chem., Int. Ed. Engl.*, 1987, **26**, 665–666.

7 A. Y. Houghton, V. A. Karttunen, W. E. Piers and H. M. Tuononen, *Chem. Commun.*, 2014, **50**, 1295–1298.

8 A. Y. Houghton, *Doctoral Thesis*, University of Calgary, 2014.

9 A. Y. Houghton, J. Hurmalainen, A. Mansikkamäki, W. E. Piers and H. M. Tuononen, *Nat. Chem.*, 2014, **6**, 983–988.

10 N. Wieprecht, I. Krummenacher, L. Wüst, M. Michel, S. Fuchs, S. Nees, M. Härterich and H. Braunschweig, *Chem. Sci.*, 2024, **15**, 12496–12501.

11 W. Haubold, J. Herdtle, W. Gollinger and W. Einholz, *J. Organomet. Chem.*, 1986, **315**, 1–8.

12 S. Biswas, I. M. Oppel and H. F. Bettinger, *Inorg. Chem.*, 2010, **49**, 4499–4505.

13 H. Braunschweig, C.-W. Chiu, J. Wahler, K. Radacki and T. Kupfer, *Chem. Eur. J.*, 2010, **16**, 12229–12233.

14 (*a*) T. Heitkemper, L. Naß and C. P. Sindlinger, *Dalton Trans.*, 2020, **49**, 2706–2714; (*b*) J. Sarcevic, T. Heitkemper and C. P. Sindlinger, *Chem. Commun.*, 2022, **58**, 246–249.

15 H. Braunschweig and T. Kupfer, *Chem. Commun.*, 2008, 4487–4489.

© 2026 The Author(s). Published by the Royal Society of Chemistry

Open Access Article. Published on 02 December 2025. Downloaded on 4/7/2026 6:27:18 PM. This article is licensed under a Creative Commons Attribution-NonCommercial 3.0 Unported Licence.

16 (*a*) V. Gutmann, *Coord. Chem. Rev.*, 1976, **18**, 225–255; (*b*) M. A. Beckett, G. C. Strickland, J. R. Holland and K. Sukumar Varma, *Polymer*, 1996, **37**, 4629–4631; (*c*) A. E. Ashley, T. J. Herrington, G. G. Wildgoose, H. Zaher, A. L. Thompson, N. H. Rees, T. Krämer and D. O'Hare, *J. Am. Chem. Soc.*, 2011, **133**, 14727–14740; (*d*) P. Erdmann and L. Greb, *Angew. Chem., Int. Ed.*, 2022, **61**, e202114550.

17 (*a*) M. J. S. Dewar and R. Dietz, *Tetrahedron Lett.*, 1959, **1**, 21–23; (*b*) M. J. S. Dewar and R. Dietz, *J. Chem. Soc.*, 1960, 1344–1347; (*c*) V. L. Arcus, L. Main and B. K. Nicholson, *J. Organomet. Chem.*, 1993, **460**, 139–147; (*d*) C. Körner, P. Starkov and T. D. Sheppard, *J. Am. Chem. Soc.*, 2010, **132**, 5968–5969; (*e*) R. Guo, K.-N. Li, B. Liu, H.-J. Zhu, Y.-M. Fan and L.-Z. Gong, *Chem. Commun.*, 2014, **50**, 5451–5454; (*f*) L. Benhamou, D. W. Walker, D.-K. Bučar, A. E. Aliev and T. D. Sheppard, *Org. Biomol. Chem.*, 2016, **14**, 8039–8043; (*g*) H. Saito, S. Otsuka, K. Nogi and H. Yorimitsu, *J. Am. Chem. Soc.*, 2016, **138**, 15315–15318; (*h*) S. Tsuchiya, H. Saito, K. Nogi and H. Yorimitsu, *Org. Lett.*, 2017, **19**, 5557–5560.

18 O. Ouadoudi, T. Kaehler, M. Bolte, H.-W. Lerner and M. Wagner, *Chem. Sci.*, 2021, **12**, 5898–5909.

19 S. Yruegas, D. C. Patterson and C. D. Martin, *Chem. Commun.*, 2016, **52**, 6658–6661.

20 M. O. Akram, J. R. Tidwell, J. L. Dutton, D. J. D. Wilson, A. Molino and C. D. Martin, *Inorg. Chem.*, 2022, **61**, 9595–9604.

21 A. Budanow, E. v. Grotthuss, M. Bolte, M. Wagner and H.-W. Lerner, *Tetrahedron*, 2016, **72**, 1477–1484.

22 Y. Ge, Q. Zhu, Y. Zhu and G. Dong, *Nat. Chem.*, 2025, DOI: 10.1038/s41557-025-01971-0.

23 T. Bischof, N. Wieprecht, S. Fuchs, L. Endres, I. Krummenacher, M. Michel, C. Mihm, H. Braunschweig and M. Finze, *Inorg. Chem.*, 2023, **62**, 21329–21335.

24 S. Yruegas and C. D. Martin, *Chem. Eur. J.*, 2016, **22**, 18358–18361.

25 A. D. Rohr, M. M. Banaszak Holl, J. W. Kampf and A. J. Ashe III, *Organometallics*, 2011, **30**, 3698–3700.

26 (*a*) P. v. R. Schleyer, C. Maerker, A. Dransfeld, H. Jiao and N. J. R. v. E. Hommes, *J. Am. Chem. Soc.*, 1996, **118**, 6317–6318; (*b*) A. C. Tsipis, *Phys. Chem. Chem. Phys.*, 2009, **11**, 8244–8261.

27 (*a*) R. Herges and D. Geuenich, *J. Phys. Chem. A*, 2001, **105**, 3214–3220; (*b*) D. Geuenich, K. Hess, F. Köhler and R. Herges, *Chem. Rev.*, 2005, **105**, 3758–3772.

28 (*a*) J. J. Eisch, N. K. Hota and S. Kozima, *J. Am. Chem. Soc.*, 1969, **91**, 4575–4577; (*b*) J. J. Eisch and J. E. Galle, *J. Am. Chem. Soc.*, 1975, **97**, 4436–4437; (*c*) J. J. Eisch, *Adv. Organomet. Chem.*, 1977, **16**, 67–109; (*d*) J. J. Eisch and J. E. Galle, *J. Organomet. Chem.*, 1977, **127**, C9–C13; (*e*) J. J. Eisch, J. E. Galle, B. Shafii and A. L. Rheingold, *Organometallics*, 1990, **9**, 2342–2349; (*f*) J. J. Eisch, *Adv. Organomet. Chem.*, 1996, **39**, 355–388.

29 P. J. Fagan, E. G. Burns and J. C. Calabrese, *J. Am. Chem. Soc.*, 1988, **110**, 2979–2981.

30 C. Fan, W. E. Piers, M. Parvez and R. McDonald, *Organometallics*, 2010, **29**, 5132–5139.

31 H. Braunschweig, J. Maier, K. Radacki and J. Wahler, *Organometallics*, 2013, **32**, 6353–6359.

32 (*a*) F. Ge, G. Kehr, C. G. Daniliuc and G. Erker, *J. Am. Chem. Soc.*, 2014, **136**, 68–71; (*b*) F. Ge, X. Tao, C. G. Daniliuc, G. Kehr and G. Erker, *Angew. Chem., Int. Ed.*, 2018, **57**, 14570–14574.

33 Y. Shoji, N. Tanaka, S. Muranaka, N. Shigeno, H. Sugiyama, K. Takenouchi, F. Hajjaj and T. Fukushima, *Nat. Comm.*, 2016, **7**, 12704.

34 Z. Wang, Y. Zhou, J.-X. Zhang, I. Krummenacher, H. Braunschweig and Z. Lin, *Chem. Eur. J.*, 2018, **24**, 9612–9621.

35 H. Kelch, S. Kachel, J. Wahler, M. A. Celik, A. Stoy, I. Krummenacher, T. Kramer, K. Radacki and H. Braunschweig, *Chem. Eur. J.*, 2018, **24**, 15387–15391.

36 F. Lindl, X. Guo, I. Krummenacher, F. Rauch, A. Rempel, V. Paprocki, T. Dellermann, T. E. Stennett, A. Lamprecht, T. Brückner, K. Radacki, G. Bélanger-Chabot, T. B. Marder, Z. Lin and H. Braunschweig, *Chem. Eur. J.*, 2021, **27**, 11226–11233.

37 T. Bischof, L. Beßler, I. Krummenacher, L. Erhard, H. Braunschweig and M. Finze, *Chem. Eur. J.*, 2023, **29**, e202300210.

38 C. Zhang, R. J. Gilliard Jr. and C. C. Cummins, *Chem. Sci.*, 2024, **15**, 17873–17880.

39 P. H. R. Oliveira, M. O. Rodrigues, C. D. G. Da Silva, J. L. Bohlen, M. Arrowsmith, A. Jayaraman, L. Lubczyk, F. Fantuzzi, E. N. da Silva Júnior and H. Braunschweig, *Angew. Chem., Int. Ed.*, 2025, e202423391.

40 For additional examples of 11B NMR shifts of borepins, see: (*a*) L. G. Mercier, W. E. Piers and M. Parvez, *Angew. Chem., Int. Ed.*, 2009, **48**, 6108–6111; (*b*) K. Schickedanz, J. Radtke, M. Bolte, H.-W. Lerner and M. Wagner, *J. Am. Chem. Soc.*, 2017, **139**, 2842–2851.

41 M. Kira and T. Iwamoto, in *The Chemistry of Organic Silicon Compounds*, ed. Z. Rappoport and Y. Apeloig, Wiley & Sons Ltd, Weinheim, 2001, vol. 3, ch. 16, pp. 854–948.

42 V. A. K. Adiraju and C. D. Martin, *Chem. Eur. J.*, 2017, **23**, 11437–11444.

43 H. Lv, K. Xiang and D.-T. Yang, *Eur. J. Org Chem.*, 2022, e202201208.

44 K.-A. Østby, G. Gundersen, A. Haaland and H. Nöth, *Dalton Trans.*, 2005, 2284–2291.

45 (*a*) CCDC 2499789: Experimental Crystal Structure Determination, 2025, DOI: 10.5517/ccdc.csd.cc12kl18; (*b*) CCDC 2499790: Experimental Crystal Structure Determination, 2025, DOI: 10.5517/ccdc.csd.cc2px7d8; (*c*) CCDC 2499791: Experimental Crystal Structure Determination, 2025, DOI: 10.5517/ccdc.csd.cc2px7f9; (*d*) CCDC 2499792: Experimental Crystal Structure Determination, 2025, DOI: 10.5517/ccdc.csd.cc2px7gb; (*e*) CCDC 2499793: Experimental Crystal Structure Determination, 2025, DOI: 10.5517/ccdc.csd.cc2px7hc; (*f*) CCDC 2499794: Experimental Crystal Structure Determination, 2025, DOI: 10.5517/ccdc.csd.cc2px7jd; (*g*) CCDC 2499795: Experimental Crystal Structure Determination, 2025, DOI: 10.5517/ccdc.csd.cc2px7kf; (*h*)

Open Access Article. Published on 02 December 2025. Downloaded on 4/7/2026 6:27:18 PM.
This article is licensed under a Creative Commons Attribution-NonCommercial 3.0 Unported Licence.

CCDC 2499796: Experimental Crystal Structure Determination, 2025, DOI: 10.5517/ccdc.csd.cc2px7lg; (*i*) CCDC 2499797: Experimental Crystal Structure Determination, 2025, DOI: 10.5517/ccdc.csd.cc2px7mh; (*j*) CCDC 2499798: Experimental Crystal Structure Determination, 2025, DOI: 10.5517/ccdc.csd.cc2px7nj; (*k*) CCDC 2499799: Experimental Crystal Structure Determination, 2025, DOI: 10.5517/ccdc.csd.cc2px7pk; (*l*) CCDC 2499800: Experimental Crystal Structure Determination, 2025, DOI: 10.5517/ccdc.csd.cc2px7ql; (*m*) CCDC 2499801: Experimental Crystal Structure Determination, 2025, DOI: 10.5517/ccdc.csd.cc2px7rm; (*n*) CCDC 2499802: Experimental Crystal Structure Determination, 2025, DOI: 10.5517/ccdc.csd.cc2px7sn; (*o*) CCDC 2499803: Experimental Crystal Structure Determination, 2025, DOI: 10.5517/ccdc.csd.cc2px7tp; (*p*) CCDC 2499804: Experimental Crystal Structure Determination, 2025, DOI: 10.5517/ccdc.csd.cc2px7vq; (*q*) CCDC 2499805: Experimental Crystal Structure Determination, 2025, DOI: 10.5517/ccdc.csd.cc2px7wr; (*r*) CCDC 2499806: Experimental Crystal Structure Determination, 2025, DOI: 10.5517/ccdc.csd.cc2px7xs; (*s*) CCDC 2499807: Experimental Crystal Structure Determination, 2025, DOI: 10.5517/ccdc.csd.cc2px7yt; (*t*) CCDC 2499808: Experimental Crystal Structure Determination, 2025, DOI: 10.5517/ccdc.csd.cc2px7zv; (*u*) CCDC 2499809: Experimental Crystal Structure Determination, 2025, DOI: 10.5517/ccdc.csd.cc2px80x; (*v*) CCDC 2499810: Experimental Crystal Structure Determination, 2025, DOI: 10.5517/ccdc.csd.cc2px81y.

© 2026 The Author(s). Published by the Royal Society of Chemistry